

# Individualised recovery trajectories of patients with impeded mobility, using distance between probability distributions of learnt graphs

Chuqiao Zhang<sup>†</sup>, Crina Grosan<sup>\*</sup>, Dalia Chakrabarty<sup>†,‡</sup>,

<sup>\*</sup> *Applied Technologies for Clinical Care  
King's College London, U.K.  
[crina.grosan@kcl.ac.uk](mailto:crina.grosan@kcl.ac.uk)*

<sup>†</sup> *Department of Mathematics  
Brunel University London  
Uxbridge UB8 3PH  
U.K.  
[joe.zhang@brunel.ac.uk](mailto:joe.zhang@brunel.ac.uk)*

<sup>‡</sup> *Department of Mathematics  
University of York  
York YO10 5DD  
U.K.  
[dalia.chakrabarty@york.ac.uk](mailto:dalia.chakrabarty@york.ac.uk)*

**Abstract:** Patients who are undergoing physical rehabilitation, benefit from feedback that follows from reliable assessment of their cumulative performance attained at a given time. In this paper, we provide a method for the learning of the recovery trajectory of an individual patient, as they undertake exercises as part of their physical therapy towards recovery of their loss of movement ability, following a critical illness. The difference between the Movement Recovery Scores (MRSs) attained by a patient, when undertaking a given exercise routine on successive instances, is given by a statistical distance/divergence between the (posterior) probabilities of random graphs that are Bayesianly learnt using time series data on locations of 20 of the patient's joints, recorded on an e-platform as the patient exercises. This allows for the computation of the MRS on every occasion the patient undertakes this exercise, using which, the recovery trajectory is drawn. We learn each graph as a Random Geometric Graph drawn in a probabilistic metric space, and identify the closed-form marginal posterior of any edge of the graph, given the correlation structure of the multivariate time series data on joint locations. On the basis of our recovery learning, we offer recommendations on the optimal exercise routines for patients with given level of mobility impairment.

**MSC2020 subject classifications:** Primary: Random graphs 60-XX; Secondary: Distance in graphs 05C12; Measures of association (correlation, canonical correlation, etc.) 62H20.

**Keywords and phrases:** Soft random geometric graphs, Probabilistic metric spaces, Statistical distance/divergence measures, Inter-graph distance, Recovery trajectories, Physical rehabilitation.

## 1. Introduction

Medicine today demands early, patient-specific diagnosis. In this paper, we put forward a tool that paves the way for predicting the recovery trajectory of an individual patient to recover their lost mobility, as they undertake physical rehabilitation. Indeed, such mobility challenges can arise in a patient because of injuries or critical illnesses, such as strokes. In fact, stroke ranks as the second most common cause of death and the third-leading cause of adult disability, [1]. Post-stroke symptoms - such as reduced mobility and discomfort caused by pain - are prevalent amongst stroke survivors. Here we introduce a new technique for reliably assessing the mobility recovery of patients with movement deficiencies, to construct each patient's recovery trajectory, as they undergo physical rehabilitation.

We learn the recovery of individual patients using a new distance/divergence between random graph variables that are learnt using the time series datasets generated as a patient repeats an exercise routine that is part of their therapy. By analysing the constructed recovery trajectories, we can predict the optimal exercise routines that are tailored to patients with varying degrees of mobility impairment. Furthermore, as our identification of an individual recovery trajectory is supplemented by the pre-therapy information about the patient's mobility status, we will in the future be able to undertake the supervised learning of the relationship between the recovery trajectory variable, and the patient's condition at the beginning of the therapy. This then will permit the all-important patient-specific and early (i.e. pre-therapy) prediction of the recovery trajectory in a prospective patient, in the context of a given therapeutic programme. Such prediction demands the establishment of the currently-absent, but requisite training set, i.e. a set of pairs of patient injury severity marker and their recovery trajectories - this set is identified in this paper, by the learning of the recovery trajectories.

There is a wide range of recovery quantification techniques reported in the literature, and yet, a standardised definition of recovery is lacking. In 2001, the World Health Organization published the International Classification of Functioning, Disability and Health (ICF) [2], as a model of classification relevant to healthcare-related domains, and this has been widely used in studies of mobility recovery of patients affected by movement-impeding conditions. This classification technique addresses three main points associated with the influence on health: body structure and function (both physical and mental); activity limitation; and restriction in participation. Indeed, ICF has worldwide usage as a reference model in the assessment of functioning, such as in the cases following traumatic injuries and stroke. The contribution of Walton (2009) [3] is also important, as they advanced 30 different primary operationalisations of recovery, (in the context of acute Whiplash Associated Disorder or WAD). Ritchie (2016) [4] summarised approaching the concept of recovery from WAD using self-reporting of relevant symptoms, (such as pain and dizziness); psychological observations such as pain catastrophising [5] and post-traumatic stress disorder symptoms. Kasch (2001) [6] and Ozegovi (2009) [7] have considered recovery as

parametrised by proxy measures such as reduction in working hours; sick leaves undertaken; and insurance claims.

In contrast to the patient-specific recovery trajectories that we report here, recovery trajectories that have been reported in the literature, refer to grouping patients by recovery. These are often pursued using Growth Mixture Modelling (GMM) and Latent Class Growth Analysis (LCGA) techniques [8–10], applied to data comprising patients’ responses to administered questionnaires [11–13], or to patient data obtained from clinics [14]. Jung and Wickrama (2008) [15] have considered LCGA and GMM techniques to identify patient groups that are homogeneously recovered; Ram and Grimm (2009) [16] summarised a four-step procedure to implement a GMM-based analysis; Panken et al. (2016) [17] undertake GMM to describe the evolution of the intensity of lower-back pain; Lee et. al (2020) [18] identified meaningful subgroups of patients who suffered from musculo-skeletal trauma by using GMM; Walton and colleagues (2021) [19] have developed the Traumatic Injuries Distress Scale to provide the magnitude and nature of risk for persistent problems in people with musculo-skeletal trauma, and have predicted the rate of recovery.

Our identification of the recovery trajectory of a patient is underlined by the computation of a statistical distance/divergence between the posterior probability of a random graph that we learn given a multivariate dataset - generated by a patient undertaking an exercise routine - and the posterior of another graph learnt given another dataset that is generated when the same patient undertakes this routine at the subsequent instance. Then recovery between the two successive undertakings of this exercise routine, is provided by the inter-graph distance that we compute. Thus, this technique demands an understanding of the random graphs that we work with here, within a Bayesian framework. We learn a random graph variable given a multivariate dataset, so that we can express the posterior probability of this random variable, conditional on said data. We write the graph posterior as contributed to by the posterior probability of each edge. In this way the graph learning here is distinct from graph learning undertaken elsewhere, as in [20, 21].

We undertake the learning of a graph variable – given the relevant data - and discuss the implementation of the inter-graph distance in Section 5, In Section 2 we discuss the advantages of our method over existing approaches used for assessing patient recovery. With the methodology discussed in Section 3, in Section 4 we present the data that we use. Discussions on methodology are followed by a presentation of our results in Section 6, We wrap up the paper with the discussions of Section 7.

## 2. Data generation

A case is made for at-home rehabilitation - enabled for example by telerehabilitation equipment that allows patients to exercise in a home environment, unencumbered by the demand of travel to a specialised rehabilitation centre, where such travel is particularly challenging for low-mobility patients. At-home

rehabilitation also offers the advantage of avoiding long waiting times and missed opportunities for early - and tailored - rehabilitative interventions. In addition, research shows that there is an increase over time in outpatient rehabilitation, as opposed to inpatient rehabilitation [22].

Here, by telerehabilitation, we refer to virtual reality-assisted rehabilitation, which is a subtopic within the analysis of human motion. It is facilitated by the use of sensors such as cameras and/or wearables. Exergames are a particular type of virtual reality platforms that are successfully used in physical rehabilitation as these exergames are designed to stimulate the repetition of a certain movement, with a focus of improving physical activity. Machine learning-based assessment of individual movement correction has been undertaken in the past [23–26], with a comprehensive review on human motion quality assessment presented in [27]. However, previous work suffer from several limitations: most of the datasets are collected from healthy individuals rather than from patients; typically, a universal benchmark is used, against which improvement/deterioration is measured for all patients; and that recovery is assessed at a time point rather than over a time interval. We offer a technique that will radically improve physiotherapy delivery via an intelligent feedback based on an individual patient’s performance and needs.

Indeed, our method of learning individualised recovery-trajectory can be integrated with telerehabilitation equipment, informing the patient and their therapists of progress on recovery made at any instance of the rehabilitation. The telerehabilitation equipment extracts detailed information about movement biomarkers and collects such information using motion sensor devices. It is the time series data on such biomarkers, generated while a patient is undertaking an exercise routine, that we use towards the construct the ion of recovery trajectories. The fast and automated generation of a reliable mobility recovery score, learnt using such recorded movement data, leads to the construction of individualised recovery trajectories. Such a construct is the first and the imperative step towards providing physiotherapist-free feedback to the patient, (as well as the therapist), on their level of recovery. We will learn such trajectories using a retrospective patient dataset, and advance recommendations regarding optimal exercise routines for patients with a given level of pre-therapy mobility deficiency. This is an important step in the attempt to automatically assess individualised physical functioning within a home environment.

### 3. Methodology

Our focus is on the development of a tool aimed at providing patients and healthcare providers with accurate and comprehensive information regarding a patient’s recovery, following engagement in a specific exergame for a predetermined number of sessions. It is imperative that information extracted on patient recovery be accurate and robust; at the same time, such information needs to be presented in a form that is easy to visualise and internalise. We propose the utilisation of a reliably-learned patient recovery trajectory as the desired tool for disseminating the sought recovery-related information.

The primary challenge lies in establishing a trustworthy, explainable, and automated learning of recovery trajectories, using the available data, namely, the time series data comprising the recorded spatial coordinates of 20 joints of the human body. These coordinates are recorded during the patient’s participation in the exergame sessions using a virtual e-platform called *MIRA Rehab* [28]. Spatial and rate coordinates of each of the 20 joints are recorded, as the  $i$ -th patient plays the  $k$ -th game, at the  $j$ -th instance.

**Definition 3.1.** *The total number of times the  $i$ -th patient plays the  $k$ -th game is  $N_{i,k}$ ; so  $j = 0, 1, \dots, N_{i,k}$ , for  $i = 1, \dots, N_p$  and  $k = 1, \dots, N_g$ .*

**Remark 3.1.** *In general, there may exist some  $k$ , such that  $N_{i,k} = 0$  since the  $i$ -th patient will not necessarily play all the available  $N_g$  games.*

As a patient executes an exergame, the location of a joint in their body changes with time - *MIRA* tracks the location of 20 joints of the patient’s skeletal frame, throughout the execution of the exergame, at regular intervals. This gives rise to a time series of patient locations. A time-dependent location of a joint in the patient’s body is given - within a pre-fixed, 3-dimensional Cartesian coordinate frame - by a 3-dimensional vector of spatial coordinates. In other words, there are three spatial coordinate variables that represent the location of each of the 20 joints, at a given time, during a patient’s execution of a given exergame.

Time derivative of each spatial coordinate of a given joint is the corresponding rate - that represents the rate of change of the location of the joint - as the patient executes the exergame, and such rate variables are also tracked by *MIRA*. However, we do not use the rates in our work.

**Definition 3.2.** *Let the three spatial coordinates of the  $s$ -th joint, recorded at time  $T = t$  during a subject playing a game, be denoted the variables  $X_s(t), Y_s(t), Z_s(t) \in \mathbb{R}$ , for  $s = 1, \dots, 20$ .*

A cartoon describing the relevance of the time series is displayed in Figure 1.

The strength of the effect, i.e. the level of recovery of movement ability, is what needs to be captured, while the  $i$ -th patient plays the  $k$ -th game in the  $j$ -th instance, compared to when they play the game at the  $j - 1$ -th instance,  $\forall j > 1; j \leq N_{i,k}$ .

**Remark 3.2.** *In our work, we understand that the recovery of movement will give rise to the differences between the “correlation structure” of the time series data recorded at the  $j$ -th instance of playing the game, and that recorded at the previous instance of playing this game. Here, the said correlation structure comprises information on the interplay - or correlation - between each pair of the 20 joints of the human body that are tracked for their location, as a subject undertakes an exergame.*

After all, a patient who is facing movement difficulties in a certain joint, will have to invoke usage of other (nearby) joints (called compensation), to perform an action that involves the former joint. Basically, there exists higher correlation

amongst pairs of (nearby) joints in such a patient, than in the case for a patient with less severe movement difficulties. Details of which joint pairs will be more strongly correlated for a given patient, depend on the nature of the movement difficulty; the undertaken task; and human anatomy. Thus, in a healthy patient who is not suffering from movement difficulties, an action that calls for the usage of a given joint, does not necessarily call for simultaneous usage of other joints, i.e. the inter-joint correlations are then lower in general, than in a patient with more severe mobility problems.

So we look at the correlation structure of locations of the monitored joints as the marker of recovery of movement. The correlation structure of a multivariate dataset is manifest in the graph of this dataset. To contextualise this to our work, we will learn a graph of the time series data that comprises values of spatial coordinates of each of 20 joints (monitored on the e-platform *MIRA*, on every instance when the  $i$ -th subject plays the  $k$ -th game), using the inter-column correlation matrix of this multivariate time series data.

### 3.1. Gist of the method used to construct recovery trajectories

We now provide a gist of the method used to construct a recovery trajectory.

- In our work, we will treat the graph as a random variable, and learn this random graph, given the correlation structure of the time series data on locations of the 20 joints, as a patient plays an exergame.
- Thus, there are 20 nodes in this random graph variable, with the location variable of a joint attached to a node. Given the inter-joint correlation of a recorded time series dataset, some nodes of the graph will be joined by a mutual edge, while the edge between some nodal-pairs will not exist in the learnt graph.
- Since the graph is random, we can define a probability distribution of this random (graph) variable, conditional on the (correlation of the) time series data generated when the  $i$ -th patient plays the  $k$ -th game, in the  $j$ -th instance.
- Then we can define a statistical distance/divergence between the probability of the graph variable learnt given the time series data generated when the  $i$ -th patient plays the  $k$ -th game in the  $j$ -th instance, and the graph learnt given the data recorded upon this patient playing the game in the  $j - 1$ -th instance. This will be done for all instances relevant to the playing of the  $k$ -th game by the  $i$ -th subject, (i.e.  $\forall j > 1; j \leq N_{i,k}$ ).
- *This distance computed for the  $j, j - 1$  graph pair is then a recovery score obtained to inform on recovery that occurred in the  $i$ -th patient, between their playing of this game in the  $j$ -th instance, and the previous instance.* Such a recovery score can be both positive and negative in general. Using this recovery score, we can generate a recovery trajectory for the  $i$ -th patient playing this  $k$ -th game.

This learning of a recovery score is seated within a highly robust mathematical technique - the implementation of which is transparent, and the method

exploits all the available information. The constructed recovery trajectory will be informative, and is a clear visual way of depicting the recovery that the  $i$ -th patient has achieved, by playing the  $k$ -th game till the  $j$ -th instance of playing.

### 3.2. Model

**Definition 3.3.** We denote the location - at time  $T = t$  - of the  $s$ -th joint (of the 20 joints tracked on the  $e$ -platform by the MIRA facility) of a given patient's body, as they play an exergame at a given instance, by the Euclidean norm  $R_s(t)$  of the  $(X_s(t), Y_s(t), Z_s(t))^T$  vector. Thus, location of the  $s$ -th joint is the variable

$$R_s(t) := \sqrt{(X_s(t))^2 + (Y_s(t))^2 + (Z_s(t))^2}.$$

Then, as the  $i$ -th patient plays the  $k$ -th exergame on the  $j$ -th instance, we use the multivariate time series data on  $X_1(t), Y_1(t), Z_1(t), X_2(t), Y_2(t), Z_2(t), \dots, X_{20}(t), Y_{20}(t), Z_{20}(t)$ , we generate the time series data on  $R_1(t), R_2(t), \dots, R_{20}(t)$ , i.e. we record the time series of the locations of each of the 20 monitored joints.

**Definition 3.4.** In our work, we define  $\mathbf{D}_{i,k,j}$  as the time series data that comprises values of  $R_1(t), \dots, R_{20}(t)$ , recorded on the  $e$ -platform MIRA at a time point  $t$ , for  $t = t_1, t_2, \dots, t_{i,k,j}^{(max)}$ , as the  $i$ -th subject plays the  $k$ -th game, in the  $j$ -th instance.

Thus, the considered time points of recording of  $R_s(t)$  values is not continuous, i.e.  $T$  is a discrete variable for us. We note that:

- the dataset  $\mathbf{D}_{i,k,j}$  has  $q_{i,k,j}^{(max)}$  rows and 20 columns, where  $t_{i,k,j}^{(max)} = (q_{i,k,j}^{(max)} - 1)\epsilon_t + t_1$ , with MIRA making observations of the 20 joints of the patient skeleton after every time interval of width  $\epsilon_t$ . Here  $q_{i,k,j}^{(max)} \in \mathbb{N}$ . Thus,  $\mathbf{D}_{i,k,j}$  is a  $q_{i,k,j}^{(max)} \times 20$ -dimensional matrix.
- Indeed, the length of time needed by a subject to play a game in one instance can differ from the length of time taken by the same or a different subject to play the same or a different game in another instance.
- Thus, the time series data recorded for different instances of playing the same game, have a different temporal coverage even for the same patient.
- We need to compute the strength of the effect that is responsible for the dataset  $\mathbf{D}_{i,k,j}$  to change into dataset  $\mathbf{D}_{i,k,j'}$ , where the temporal coverage of the two datasets is not necessarily the same, i.e.  $t_{i,k,j}^{(max)} \neq t_{i,k,j'}^{(max)}$  in general, for  $j \neq j'$ ;  $j, j' = 1, \dots, N_{i,k}$ . This effect is caused by the recovery of movement that the  $i$ -th patient has undergone, between them executing the  $k$ -th game in the  $j$ -th instance and the  $j'$ -th instance.

**Definition 3.5.** As motivated above, we parametrise the strength of the effect that causes  $\mathbf{D}_{i,k,j}$  to change into dataset  $\mathbf{D}_{i,k,j'}$ , by a distance/divergence between the probability of the graph learnt given the inter-joint correlation matrix  $\Sigma_{(i,k,j)}^{(C)}$  of the dataset  $\mathbf{D}_{i,k,j}$ , and the graph learnt given the inter-joint correlation matrix of the dataset  $\mathbf{D}_{i,k,j-1}$ .

**Definition 3.6.** We standardise the value of  $R_s(t)$  using the mean and standard deviation of the sample:  $\{r_s^{(i,k,j)}(t_1), r_s^{(i,k,j)}(t_2), \dots, r_s^{(i,k,j)}(t_{i,k,j}^{(max)})\}$  that is recorded when the  $i$ -th patient plays the  $k$ -th exergame on the  $j$ -th instance, with  $r_s^{(i,k,j)}(t)$  denoted the value attained by the location variable  $R_s(t)$ , at time  $T = t$ . Here, the estimates of the sample mean  $\bar{r}_s^{(i,k,j)}$  and sample standard deviation  $\zeta_{r_s}^{(i,k,j)}$  are given as:

$$\bar{r}_s^{(i,k,j)} := \frac{\sum_{t=t_1}^{t_{i,k,j}^{(max)}} r_s^{(i,k,j)}(t)}{q_{i,k,j}^{(max)}} \quad \zeta_{r_s}^{(i,k,j)} := \sqrt{\frac{\sum_{t=t_1}^{t_{i,k,j}^{(max)}} \left( r_s^{(i,k,j)}(t) - \bar{r}_s^{(i,k,j)} \right)^2}{(q_{i,k,j}^{(max)} - 1)}}.$$

We undertake such standardisation  $\forall s = 1, \dots, 20$ .

**Remark 3.3.** The dataset generated by the standardised joint location values is from now on, still referred to as  $\mathbf{D}_{i,k,j}$ , i.e. we do not introduce a new notation for the dataset comprising the standardised data.

Values attained by the random variable  $R_s(t)$ , comprise the  $q$ -th row and the  $s$ -th column of the dataset  $\mathbf{D}_{i,k,j}$ , (for  $t = q\epsilon_t$ ). The fact that the number of rows of the dataset  $\mathbf{D}_{i,k,j}$  and the dataset  $\mathbf{D}_{i,k,j'}$  are unequal, does not affect our Bayesian learning of the random graph variable that is realised given either data set, and therefore, the inter-graph distance is robust to the difference in the number of rows in either dataset.

### 3.3. Learning/estimation of the correlation matrix

**Definition 3.7.** Let the correlation matrix of dataset  $\mathbf{D}_{i,k,j}$  be  $\Sigma_{i,k,j}^{(C)} = [\rho_{s,s'}]$ , where  $\rho_{s,s'}$  is the correlation between the random variables  $P_s^{(i,k,j)}$  and  $P_{s'}^{(i,k,j)}$ , with the  $q$ -th recorded (by MIRA) value of  $P_s^{(i,k,j)}$  realised at time  $T = t = q\epsilon_t$ , as  $r_s^{(i,k,j)}(t)$ , when the  $i$ -th patient executes the  $k$ -th game in the  $j$ -th instance. Here,  $s, s' = 1, \dots, 20$ .

Indeed, in our recorded data  $\mathbf{D}_{i,k,j}$ , realisation of random variable  $P_s^{(i,k,j)}$  recorded at  $T = t$ , concurs with the realisation of the variable  $R_s^{(i,k,j)}(t)$ ,  $\forall t = t_1, \dots, t_{i,k,j}^{(max)}$ .

The following enumerates our addressing of the problem of learning/estimating the correlation matrix  $\Sigma_{i,k,j}^{(C)}$ .

- We could undertake the learning of each correlation element directly within the inferential scheme that we could invoke, such as Markov Chain Monte Carlo (or MCMC) based algorithms. However, there are  $(20 \times 20 - 20)/2 = 190$  distinct off-diagonal elements of this symmetric correlation matrix, and learning 190 (correlation) parameters using MCMC is a daunting - and in fact, an impossibly daunting - task.

- It may appear possible to undertake parametrisation of this correlation matrix using a covariance kernel, that takes as its input a difference between the values of an input variable, and produces the correlation between the outputs generated at these inputs. However, there is no relevant variable that could serve as such an “input” variable. The index of a joint in the human body - the location of which is monitored at a given time point as the patient plays an exergame - is merely nominal, and can be arbitrarily assigned to a joint, rendering the difference between indices of two such joints bereft of any useful interpretation.
- Then we cannot learn any element of the correlation matrix  $\Sigma_{i,k,j}^{(C)}$ ; we can therefore only estimate each element, using the sample of values of the location variable  $P_s^{(i,k,j)}$  and that of  $P_{s'}^{(i,k,j)}$ , as included across the  $q_{i,k,j}^{(max)}$  rows of this time series dataset. We compute the estimate of the Pearson correlation coefficient.

**Definition 3.8.** *The unbiased estimator  $\hat{\rho}_{s,s'}$  of the correlation  $\rho_{s,s'}$  between variables  $P_s^{(i,k,j)}$  and  $P_{s'}^{(i,k,j)}$  as:*

$$\hat{\rho}_{s,s'} = \frac{\sum_{i=t_1}^{t_{i,k,j}^{(max)}} r_s^{(i,k,j)}(t) r_{s'}^{(i,k,j)}(t)}{q_{i,k,j}^{(max)} - 1},$$

recalling that the data on  $P_s^{(i,k,j)}$  is standardised. This holds for  $s, s' = 1, \dots, 19$ .

Then the inter-column correlation matrix estimated in data  $\mathbf{D}^{(i,k,j)}$  is  $\hat{\Sigma}_{i,k,j}^{(C)} = [\hat{\rho}_{s,s'}]$ .

**Definition 3.9.** *The partial correlation  $\psi_{s,s'}$  between variables  $P_s^{(i,k,j)}$  and  $P_{s'}^{(i,k,j)}$  is computed using the estimated  $\theta_{s,s'}$ , given the precision matrix  $\Theta_{i,k,j} = [\theta_{s,s'}] := (\Sigma_{i,k,j}^{(C)})^{-1}$ . In fact, the inter-column partial correlation matrix of dataset  $\mathbf{D}_{i,k,j}$  is  $\Psi_{i,k,j}^{(C)} = [\psi_{s,s'}]$ , for  $s, s' = 1, \dots, 20$ , where*

$$\psi_{s,s'} = -\frac{\theta_{s,s'}}{\sqrt{\theta_{s,s} \theta_{s',s'}}}, s \neq s', \text{ and we have } \psi_{s,s} = 1 \text{ for } s = s'. \quad (3.1)$$

### 3.4. Outlining graph learning & inter-graph distance computation

1. Once the partial correlation  $\psi_{s,s'}$  between variables  $P_s^{(i,k,j)}$  and  $P_{s'}^{(i,k,j)}$  is computed, we learn the value of the (binary) edge  $G_{s,s'}$  variable that joins the  $s$ -th and  $s'$ -th nodes, (i.e. learn if  $g_{s,s'}$  is 1, or is instead 0), given  $\psi_{s,s'}$ . We recall that random variables  $P_s^{(i,k,j)}$  and  $P_{s'}^{(i,k,j)}$  sit at the  $s$ -th and  $s'$ -th nodes respectively. In our Bayesian setting, we perform this edge learning by computing the posterior probability of this edge, conditional on  $\psi_{s,s'}$ , for each relevant  $s, s'$  pair, i.e.  $\forall s, s'; s < s'; s = 1, \dots, 19$ .

2. Thus, the edge between the  $s$ -th and  $s'$ -th nodes is modelled to be affected by the partial correlation between *only* the variables  $P_s^{(i,k,j)}$  and  $P_{s'}^{(i,k,j)}$ , while values of all other variables are held as fixed. Another possibility would be to learn  $G_{s,s'}$  as conditional on the correlation between  $P_s^{(i,k,j)}$  and  $P_{s'}^{(i,k,j)}$ , computing which does not demand that all other variables be held fixed.
3. In this work, we write the edge probability of  $G_{s,s'}$  conditional on the data - namely, the partial correlation  $\psi_{s,s'}$  between the nodes that this edge joins - as  $m(G_{s,s'}|\psi_{s,s'})$ . We will identify a closed-form expression for this conditional probability ( $m(G_{s,s'}|\psi_{s,s'})$ ) below (in Equation 3.2). We will include the edge between the  $s$ -th and  $s'$ -th nodes, only if the edge probability exceeds a chosen ‘‘cut-off’’ probability  $\tau \in [0, 1]$ , i.e.  $g_{s,s'} = 1$ , if  $m(G_{s,s'} = g_{s,s'}|\psi_{s,s'}) \geq \tau$ .
4. Now, to check if  $m(G_{s,s'}|\psi_{s,s'}) \geq \tau$ , we need to compute  $m(G_{s,s'} = g_{s,s'}|\psi_{s,s'})$ , and to compute this posterior probability, we need to know the value  $g_{s,s'}$  of the edge variable  $G_{s,s'}$ . We recognise the problem of learning  $g_{s,s'}$  from the posterior probability of  $G_{s,s'}$  given the data, as a problem in Bayesian inference. We sample  $g_{s,s'}$  from this edge posterior, the closed-form expression of which is available, as we have stated above. We undertake Rejection Sampling to sample from the edge posterior  $m(G_{s,s'} = g_{s,s'}|\psi_{s,s'})$ , for all relevant nodal pairs. As in any implementation of Bayesian inference, we will then have  $N$  sampled  $g_{s,s'}$  values, and the edge posterior at each sampled edge value.
  - The set of posterior values for all relevant edge variables will define the posterior of the graph variable, given the partial correlation matrix of one dataset, and we will compute the inter-graph distance/divergence between the graph posterior given this dataset and that given another, as per Definition 3.16/3.17.
  - The set of sampled edge values will be employed to compute an estimate of the edge posterior probability, which if  $\geq \tau$ ,  $G_{s,s'}$  is set to 1 in a realisation of the graph variable at a chosen  $\tau$ ; else we set  $G_{s,s'}$  to 0. This is discussed in Definition 3.14.
5. One question remains unanswered still: what is the justification behind using  $m(G_{s,s'} = g_{s,s'}|\psi_{s,s'}) \geq \tau$  to check for the existence of an edge? The answer is that this inequality follows from our modelling of the random graph as a Random Geometric Graph, (or RGG), any edge of which is a probability. Such an RGG is manifest if we draw the RGG in a probabilistic metric space. We discuss such an RGG next.

### 3.5. Random graph variable

The graph of the  $q_{i,k,j}^{(max)} \times 20$ -dimensional dataset  $\mathbf{D}_{i,k,j}$ , is defined on the vertex set  $\mathbf{V} = \{P_1^{(i,k,j)}, \dots, P_{20}^{(i,k,j)}\}$ . There are no self-loops allowed in this graph

and the edges form independently of each other. This graph is drawn using the  $20 \times 20$ -dimensional partial correlation matrix  $\Psi_{i,k,j}^{(C)}$ , any element of which can be computed by Equation 3.1. As stated above, in this work, the random graph variable is a Random Geometric Graph [29–32] drawn in a probabilistic metric space [33].

**Definition 3.10.** *A Random Geometric Graph (RGG) is s.t. an edge exists between a pair of nodes, if and only if, the distance between the nodes falls below a pre-fixed cutoff or threshold  $\tau$ .*

Therefore, in an RGG, the affinity function between the pair of variables that are attached to a pair of nodes - where the affinity is complimentary to the inter-nodal distance function - exceeds or equals  $\tau$  to ensure that the mutual edge exists; else the edge is absent.

**Definition 3.11.** *In a probabilistic metric space, to any pair of points in this space, we can assign a probability distribution of a non-negative function of this pair of points, s.t. the distribution is over non-negative support.*

Just as a non-negative distance can be assigned to a pair of points in a metric space, in a probabilistic metric space, a probability distribution with non-negative support is assigned to a pair of points<sup>1</sup>.

Thus, any edge of the RGG variable drawn in probabilistic metric space, is a probability. As the (probabilistic) distance between variables  $P_s^{(i,k,j)}$  and  $P_{s'}^{(i,k,j)}$  increases, there is a decrease in the probability that an edge will join the nodes that these variables sit at. In other words, as the value of the (complimentary) affinity function between  $P_s^{(i,k,j)}$  and  $P_{s'}^{(i,k,j)}$  decreases, there is an decrease in the edge probability. Similarly, increasing affinity implies edge probability is increasing. The affinity is then intuited to be given by the probability of the edge variable  $G_{s,s'}$ . Then as in an RGG, we demand that only if the affinity between  $P_s^{(i,k,j)}$  and  $P_{s'}^{(i,k,j)}$  exceeds a chosen cutoff  $\tau$  - i.e. only if edge probability exceeds  $\tau$  - the edge exists between the  $s$ -th and  $s'$ -th nodes.

### 3.6. Edge posterior & samples generated from it

Here, this probabilistic distance between any two nodes of the RGG is a measure of the *intra-graph* distance function, while our interest in this application is in the distance/divergence between a pair of RGGs learnt given two distinct time series (on joint locations) datasets, where the *inter-graph* distance/divergence is defined between posterior probability of a graph variable learnt given one dataset, and that learnt given another data. The posterior of the graph is in turn

<sup>1</sup>Formally, a probabilistic metric space is a triple comprising: the sample space that hosts random variables; a probabilistic distance function between any two points in this space; and a triangle function that underwrites this distance function by assuring its adherence to the triangle rule. Said probabilistic distance function is a probability distribution over non-negative support.

contributed to by the posterior probability of each edge variable that connects each nodal pair of this graph.

We now enumerate steps to the achievement of this edge posterior.

- As motivated by [34], the first step in the formulation of the edge marginal is to model the probability density function of the partial correlation  $\psi_{s,s'}$ , as  $\mathcal{N}(g_{s,s'}, v_{s,s'})$ , where  $v_{s,s'}$  is the variance parameter relevant to this  $(s, s')$ -th nodal pair.
- Then, in Bayes rule, we input this density of the (observable) partial correlation conditional on the edge and variance parameter, and use weak priors on the two model parameters - Bernoulli(0.5) on  $G_{s,s'}$  and Uniform on  $v_{s,s'}$  - to write the joint posterior probability density of  $G_{s,s'}$  and  $v_{s,s'}$ , given partial correlation  $\psi_{s,s'}$ .
- This joint posterior is then proportional to:  $(2\pi v_{s,s'})^{-1/2} \exp(-(g_{s,s'} - \psi_{s,s'})^2/2v_{s,s'})$ , since the priors are constants with respect to the parameters.
- We then marginalise the variance parameter out of this joint posterior by integrating this joint over values of  $v_{s,s'}$  in the interval  $(0, u]$  for a chosen  $u > 0$ . We provide one model for the edge marginal posterior probability given the partial correlation between  $P_s^{(i,k,j)}$  and  $P_{s'}^{(i,k,j)}$  by choosing  $u = 1$ , where  $(0, 1]$  is shown as an exhaustive set for  $v_{s,s'}$  to take values in.
- The resulting integral - i.e. the edge marginal posterior - is given as:

$$m(G_{s,s'}|\psi_{s,s'}) = K \left[ \sqrt{\frac{2}{\pi}} \exp\left(\frac{-(S_{s,s'})^2}{2}\right) - S_{s,s'} \operatorname{erfc}\left(\frac{S_{s,s'}}{\sqrt{2}}\right) \right],$$

where  $S_{s,s'} := |G_{s,s'} - |\psi_{s,s'}|| \in [0, 1]$ .

(3.2)

Here the complementary error function  $\operatorname{erfc}(\cdot) = 1 - \operatorname{erf}(\cdot)$ , and  $K > 0$  is an identifiable constant.

**Definition 3.12.** *Modelling edges to form independently of each other, the posterior probability of the random graph variable  $\mathcal{G}_{i,k,j}(\mathbf{V})$ , conditional on the partial correlation of data  $\mathbf{D}_{i,k,j}$ , is the product over all relevant  $s, s'$  pairs, of the conditional edge marginal given in Equation 3.2:*

$$\begin{aligned} \pi(\mathcal{G}_{i,k,j}(\mathbf{V})|\mathbf{D}_{i,k,j}) &= \prod_{s < s'; s=1}^{N-1} m(G_{s,s'}|\psi_{s,s'}) \\ &= K / \prod_{s < s'; s=1}^{N-1} \left[ \sqrt{\frac{2}{\pi}} \exp\left(\frac{-(S_{s,s'})^2}{2}\right) - S_{s,s'} \operatorname{erfc}\left(\frac{S_{s,s'}}{\sqrt{2}}\right) \right] \quad , \quad (3.3) \end{aligned}$$

It is from the closed-form marginal posterior probability  $m(G_{s,s'}|\psi_{s,s'})$  (of edge  $G_{s,s'}$ ) given in Equation 3.2, that we generate  $N$  samples of  $G_{s,s'}$  using Rejection Sampling. This sample is:

$$\xi_{s,s'} := \{g_{s,s'}^{(1)}, \dots, g_{s,s'}^{(N)}\}.$$

Here,  $g_{s,s'}^{(r)}$  can be 1 or 0,  $\forall r = 1, \dots, N$ . This is undertaken  $\forall s, s'; s < s'; s = 1, \dots, 19$ . Details of this undertaken Rejection sampling are given in Section 5.2.

Posterior of the graph variable  $\mathcal{G}_{i,k,j}(\mathbf{V})$  constructed using the  $r$ -th sampled value of  $G_{s,s'}$ , for all relevant  $s, s'$ -th pairs - given data  $\mathbf{D}_{i,k,j}$  - is denoted  $\pi(\mathcal{G}_{i,k,j}(\mathbf{V})|\mathbf{D}_{i,k,j})^{(r)}$ , where  $r = 1, 2, \dots, N$ . We use  $\pi(\mathcal{G}_{i,k,j}(\mathbf{V})|\mathbf{D}_{i,k,j})^{(1)}, \dots, \pi(\mathcal{G}_{i,k,j}(\mathbf{V})|\mathbf{D}_{i,k,j})^{(N)}$  for the computation of the inter-graph distance/divergence, (discussed in Section 3.8).

### 3.7. Realisation of the graph variable at a chosen $\tau$

While we will compute the inter-graph distance/divergence, we will also visualise the graph generated using Rejection Sampling, at a given choice of  $\tau$  - constructed using Definition 3.14 (that invokes Definition 3.13).

**Definition 3.13.** *The relative frequency of edge variable  $G_{s,s'}$  in the sample  $\xi_{s,s'}$  is  $\nu_{s,s'} = \sum_{n=1}^N g_{s,s'}^{(n)} / N$ .*

Then  $\nu_{s,s'}$  estimates  $m(G_{s,s'}|\psi_{s,s'})$  in the sample  $\{g_{s,s'}^{(1)}, g_{s,s'}^{(2)}, \dots, g_{s,s'}^{(N)}\}$ .

**Definition 3.14.** *In our work, the realisation  $\mathcal{G}_{\mathbf{V},m}(\Psi, \tau)$  of the graph variable is learnt at the cutoff  $\tau$ ,*

- on the vertex set  $\mathbf{V}$ ; using the edge probability  $m(\cdot)$  defined in Equation 3.2; for the inter-column partial correlation matrix  $\Psi_{i,k,j}^{(C)}$  of the dataset  $\mathbf{D}_{i,k,j}$ ; and for the chosen cut-off  $\tau$ ,
- where edge between the  $s$ -th and  $s'$ -th nodes exists, (i.e.  $g_{s,s'} = 1$ ) if and only if  $\nu_{s,s'} \geq \tau$ ,  $\forall s, s'; s < s'; s = 1, \dots, 19$ . Here,  $\nu_{s,s'}$  is defined in Definition 3.14.

### 3.8. Inter-graph distance formalisation

A statistical distance or divergence can be computed between the posterior probability of the graph variable conditional on the time series data  $\mathbf{D}_{i,k,j}$ , and that given data  $\mathbf{D}_{i,k,j}$ . The Hellinger distance is an example of such a statistical distance while the Kullbeck Leibler divergence can also be computed.

**Definition 3.15.** *The squared Hellinger distance between the probability density  $p_1(x)$  and another density  $p_2(x)$  (for  $x \in \mathcal{X}$ ) is:*

$$D_H^2(p_1, p_2) = \int_{\mathcal{X}} (\sqrt{p_1(x)} - \sqrt{p_2(x)})^2 dx.$$

**Definition 3.16.** *Recalling that the graph posterior probability is computed at each of the  $N$  number of samples generated using Rejection Sampling, for the*

random graph variables learnt given data  $\mathbf{D}_{i,k,j}$  and  $\mathbf{D}_{i,k,j'}$ , the squared discretised Hellinger distance between their posterior probabilities is

$$D_H^2(\mathcal{G}_{i,k,j}(\mathbf{V}), \mathcal{G}_{i,k,j'}(\mathbf{V})) = \frac{\sum_{r=1}^N \left( \sqrt{\pi(\mathcal{G}_{i,k,j}(\mathbf{V})|\mathbf{D}_{i,k,j})^{(r)}} - \sqrt{\pi(\mathcal{G}_{i,k,j'}(\mathbf{V})|\mathbf{D}_{i,k,j'})^{(r)}} \right)^2}{N}, \quad (3.4)$$

where  $\pi(\mathcal{G}_{i,k,j}(\mathbf{V})|\mathbf{D}_{i,k,j})^{(r)}$  is the graph posterior given the data  $\mathbf{D}_{i,k,j}$ , computed with the  $r$ -th sample of the edges of the graph,  $\forall r = 1, \dots, N$ .

We compute the Hellinger distance  $D_H(\mathcal{G}_{i,k,j}(\mathbf{V}), \mathcal{G}_{i,k,j-1}(\mathbf{V}))$  between graph posterior given the data  $\mathbf{D}_{i,k,j}$  and that given data  $\mathbf{D}_{i,k,j-1}$ , where these datasets are generated by the  $i$ -th patient playing the  $k$ -th exergame, in the  $j$ -th and  $j-1$ -th instances, for all  $i$  and  $k$  relevant in our data to  $j > 1$ , i.e. for all patients who play an exergame multiple times.

**Definition 3.17.** *Alternatively, we can compute the Kullbeck-Leibler divergence between the posteriors of the graphs  $\mathcal{G}_{i,k,j}(\mathbf{V})$  and  $\mathcal{G}_{i,k,j-1}(\mathbf{V})$ , given the data  $\mathbf{D}_{i,k,j}$  and  $\mathbf{D}_{i,k,j-1}$ , as:*

$$D_{KL}(\mathcal{G}_{i,k,j}(\mathbf{V}), \mathcal{G}_{i,k,j-1}(\mathbf{V})) = \sum_{r=1}^N \pi(\mathcal{G}_{i,k,j}(\mathbf{V})|\mathbf{D}_{i,k,j})^{(r)} \log \left( \frac{\pi(\mathcal{G}_{i,k,j}(\mathbf{V})|\mathbf{D}_{i,k,j})^{(r)}}{\pi(\mathcal{G}_{i,k,j-1}(\mathbf{V}, \tau)|\mathbf{D}_{i,k,j-1})^{(r)}} \right), \quad (3.5)$$

where the posterior of the random graph variable is computed given the datasets generated by the  $i$ -th subject playing the  $k$ -th game on successive instances, i.e. at the  $j-1$ -th and  $j$ -th instances, for  $j = 2, \dots, N_{i,k}^{(max)}$ .

The kind of random graphs that we have learnt in our current work, could be considered to fall within the broad class of Inhomogeneous Random Graphs [35, 36].

### 3.9. Construction of recovery trajectories

The posterior probability of a random graph variable - given time-series datasets on joint locations generated by a patient playing a given exergame at successive instances - will be utilised to compute the inter-graph distance/divergence between adjacent instances. Such an inter-graph distance computed between the  $j$ -th and the  $j-1$ -th instances of the  $i$ -th patient playing the  $k$ -th game will inform on the movement recovery attained by this patient between these two instances of playing the game. (Here  $j = 2, \dots, N_{i,k}^{(max)}$ ).

**Definition 3.18.** *Movement recovery is treated as the difference between the ‘‘Mobility Recovery Score’’ or  $MRS_{i,k}(j)$  attained by the  $i$ -th patient when playing the  $k$ -th exergame in the  $j$ -th instance, and the score  $MRS_{i,k}(j-1)$*

attained in the  $j - 1$ -th instance of playing this game. We model the MRS as proportional to the inter-graph distance/divergence between the random graph variables learnt given datasets  $\mathbf{D}_{i,k,j}$  and  $\mathbf{D}_{i,k,j-1}$ . We define the constant of proportionality to be unity, since we are defining the MRS here.

When we compute the MRS using the Hellinger distance, we denote the score as  $\mathcal{MRS}_{i,k}^{(Hell)}(\cdot)$ . On the other hand, when we use the KL-divergence to give the value of the MRS, we denote the score  $\mathcal{MRS}_{i,k}^{(KL)}(\cdot)$ . We can model the difference between  $\mathcal{MRS}_{i,k}^{(Hell)}(j)$  and  $\mathcal{MRS}_{i,k}^{(Hell)}(j - 1)$  as proportional to the Hellinger distance between the graph variables learnt given the time series data  $\mathbf{D}_{i,k,j}$  and  $\mathbf{D}_{i,k,j-1}$  respectively, i.e.

$$\mathcal{MRS}_{i,k}^{(Hell)}(j) - \mathcal{MRS}_{i,k}^{(Hell)}(j - 1) \propto D_H(\mathcal{G}_{i,k,j}(\mathbf{V}), \mathcal{G}_{i,k,j'}(\mathbf{V})),$$

where we advance the value of 1 for the proportionality constant, as stated above.

**Remark 3.4.** Now,  $\mathcal{MRS}_{i,k}(j) - \mathcal{MRS}_{i,k}(j - 1)$  is the difference in the MRS between the  $j$ -th and  $j - 1$ -th instances of playing the  $k$ -th game. So this difference is the same as the rate of change of MRS with respect to instance of playing, at the  $j - 1$ -th instance of playing this game. Thus, the  $i$ -th patient's rate of change of mobility at the  $j$ -th instance of playing the  $k$ -th game, using Hellinger distance is  $D_H(\mathcal{G}_{i,k,j}(\mathbf{V}), \mathcal{G}_{i,k,j'}(\mathbf{V}))$ , such that their improvement score - or MRS - at this  $j$ -th instance of playing this game is

$$\mathcal{MRS}_{i,k}^{(Hell)}(j) = D_H(\mathcal{G}_{i,k,j}(\mathbf{V}), \mathcal{G}_{i,k,j'}(\mathbf{V})) + \mathcal{MRS}_{i,k}^{(Hell)}(j - 1),$$

where  $j = 2, \dots, N_{i,k}^{(max)}$ .

Again, when using the KL-divergence to compute the inter-graph distance, we set the improvement score of the  $i$ -th patient at the  $j$ -th instance of playing the  $k$ -th game to be:

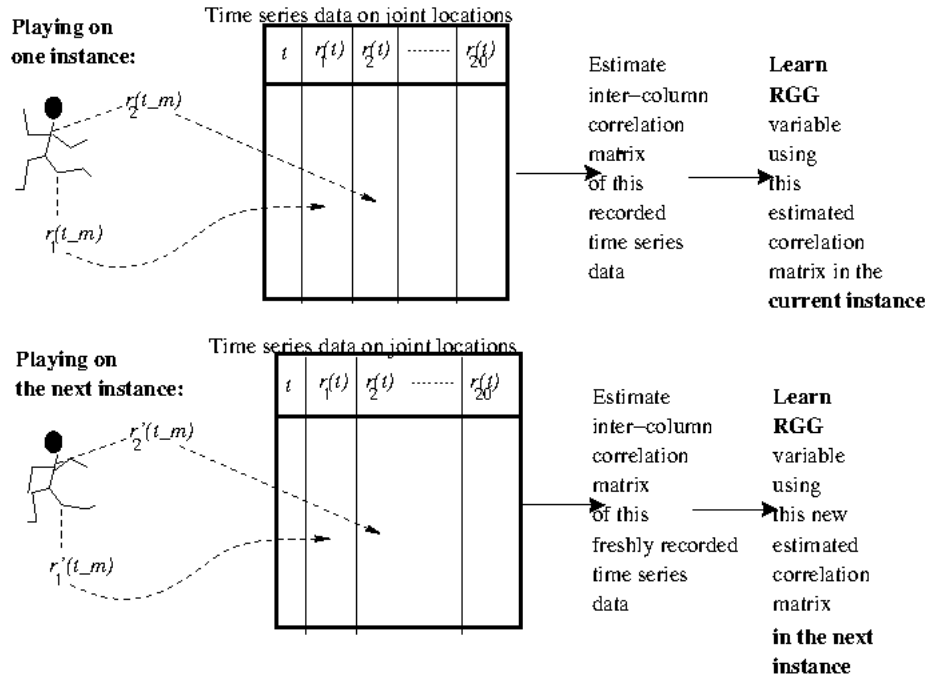
$$\mathcal{MRS}_{i,k}^{(KL)}(j) = D_{KL}(\mathcal{G}_{i,k,j}(\mathbf{V}), \mathcal{G}_{i,k,j'}(\mathbf{V})) + \mathcal{MRS}_{i,k}^{(KL)}(j - 1),$$

with  $j = 2, \dots, N_{i,k}^{(max)}$ .

We set  $\mathcal{MRS}_{i,k}^{(\cdot)}(1) = 0$  and plot  $\mathcal{MRS}_{i,k}^{(\cdot)}(j)$  against  $j$ .

**Definition 3.19.** The variation of  $\mathcal{MRS}_{i,k}^{(\cdot)}(j)$  with  $j$  constitutes the recovery trajectory for the  $i$ -th patient, as they play the  $k$ -th game.

Since the posterior of a random graph variable, given the time series data on the 20 joint locations is the joint posterior of all edges of the RGG with  $(20^2 - 20)/2 = 190$  nodes, the posterior of the graph variable  $\mathcal{G}_{i,k,j}(\mathbf{V})$  is a small number. Therefore, the distance/divergence between the posterior of random graph variable  $\mathcal{G}_{i,k,j}(\mathbf{V})$  given data  $\mathbf{D}_{i,k,j}$ , and of  $\mathcal{G}_{i,k,j-1}(\mathbf{V})$  given data  $\mathbf{D}_{i,k,j-1}$ , is typically a small number. In fact, the divergence values are smaller than the distance values. To avoid working with such small numbers, we scale the posterior



Compute distance/divergence between:

$$\begin{aligned}
 & \text{posterior(RGG learnt given (correlation of) data generated by playing in the next instance)} - \\
 & \text{posterior(RGG learnt given (correlation of) data generated by playing in the current instance)} \\
 & = \text{Mobility Recovery Score in the next instance} - \\
 & \text{Mobility Recovery Score in the current instance.}
 \end{aligned}$$

Fig 1: A cartoon of the basic framework of the method. The same patient plays a given exergame on successive instances - resulting in two successively recorded time series data on the locations of the 20 monitored joints in their body. The spatial coordinates of the three-dimensional location vector are periodically recorded on the e-platform *MIRA*. The Euclidean norm of this vector then gives the location of a joint, at a time point when a recording is done by *MIRA*. Thus, a time series (on joint location) data is produced as the patient plays this exergame. The inter-column correlation matrix of this data is estimated, and this estimated correlation used to learn a random graph variable - which is a Random Geometric Graph variable (or an RGG variable) in our work. Again, when this patient plays this exergame on the next instance, a new time series data is recorded; its inter-column correlation matrix estimated; and the RGG of this data is then learnt. A statistical distance/divergence measure between the posterior probabilities of the RGGs learnt given the (correlation of the) two datasets, is set proportional to the difference between the Mobility Recovery Scores attained (by this patient playing this exergame) at the next instance, and at the current instance.

of any random graph variable, learnt using a dataset that we consider in our work, by  $10^{15}$ , when computing Hellinger distance between any pair of graph posteriors, given any pair of time series datasets. Again, when computing the Kullback Leibler divergence, we scale any such posterior value with  $10^{25}$ .

We have confirmed the robustness of the undertaken Rejection sampling, to variation in the proposal density. In Section 6.3, we demonstrate recovery trajectories that are learnt using a Bernoulli proposal, as well as a Uniform proposal.

#### 4. Data

The data was collected while a cohort of patients - who were suffering mobility deficiencies due to a stroke and were undergoing physical rehabilitation - played exergames on the *MIRA* platform. This is a virtual reality platform and the users interact with the exergames via a Kinect motion sensor camera. Data consists of recordings of the three spatial coordinates ( $X, Y, Z$ ) of 20 joints of the skeletal structure of the patient who is playing an exergame. An exergame engages the subject in the execution of a certain physical exercise or a combination of two or more exercises (for instance: knee flexion; knee extension; lateral flexion; shoulder abduction; frontal flexion; hip abduction; full body turn, etc). The execution of any exergame is captured as a sequence of frames, with each frame capturing the three spatial coordinates of each of the 20 considered joints. This translates into a sequence over the time taken to play the exergame, or a time series - in each dimension of each of the 20 considered joints. In our work, we reduce the dimensionality of this recorded time series from 60 to 20, by agglomerating the three spatial coordinates to the location  $R := \sqrt{X^2 + Y^2 + Z^2}$ . Typically, a patient's movement is recorded for 3 minutes at a frequency of 30Hz. In the cohort, 13 patients have played various games, with multiple repetitions of each exergame, and at various levels of difficulty, as presented in Figure 2. Overall, 2,661 sessions were recorded, and these are not uniformly distributed amongst patients and exergames.

Table 1 presents a snippet of the data available for an individual patient in the cohort. This example patient is one with reference 3071 in our database. The table contains the time series data on the 20 joint locations while the patient played an exergame called *Airplane* that involves physical exercises such as elbow flexion; movement of the arm; moving the shoulder; moving the spine and moving the hip. In Table 1, we present the first few lines of the values of locations of some of the 20 joints in the patient's body, as monitored on the e-platform *MIRA*, as this patient (with identity reference ID3071) played *Airplane*.

The e-platform outputs several statistics at the end of each session (or undertaken exergame), such as moving time in exercise; still time; average correct answer reaction time; average incorrect answer reaction time; etc., as well as the points gained for each exergame played. These inbuilt points are expected to function as an indicator of patient performance in executing the exergame

$\forall j = 2, \dots, N_{i,k}^{(max)}$ .  
 /\* Start learning recovery trajectory for  $i$ -th patient playing the  $k$ -th exergame, on the  $j$ -th instance \*/  
 Spatial coordinate values  $x_s^{(i,k,j)}(t), y_s^{(i,k,j)}(t), z_s^{(i,k,j)}(t)$  of the  $s$ -th joint recorded at  $t = t_1, t_2, \dots, t_{i,k,j}^{(max)}$ , by MIRA, as this exergame is played;  $s = 1, \dots, 20$ .  
**for**  $t \leftarrow 1$  **to**  $t_{i,k,j}^{(max)}$  **increment by 1, do**  
     **for**  $s \leftarrow 1$  **to** 20 **increment by 1, do**  
         Compute location value  $r_s^{(i,k,j)}(t)$  of the  $s$ -th joint at time  $T = t$ , as:  
          $r_s^{(i,k,j)}(t) = \sqrt{(x_s^{(i,k,j)}(t))^2 + (y_s^{(i,k,j)}(t))^2 + (z_s^{(i,k,j)}(t))^2}$ .  
     **end**  
**end**  
 Gives rise to  $t_{i,k,j}^{(max)} \times 20$ -dimensional time series (on joint location) dataset.  
 Estimate  $20 \times 20$ -dimensional inter-column correlation matrix  $\Sigma_{i,k,j}^{(C)}$  as per Definition 3.8.  
 Compute partial correlation matrix  $\Psi_{i,k,j}^{(C)}$  using  $\Sigma_{i,k,j}^{(C)}$  as per Definition 3.9.  
**for**  $r \leftarrow 1$  **to**  $N = 50,000$  **increment by 1, do**  
     **for**  $s \leftarrow 1$  **to** 19 **increment by 1, do**  
         **for**  $s' \leftarrow s + 1$  **to** 20 **increment by 1, do**  
             Given  $s, s'$ -th element of  $\Psi_{i,k,j}^{(C)}$ , sample  $g_{s,s'}$  from edge marginal  $m(G_{s,s'} | \Psi_{i,k,j}^{(C)})$  given in Equation 3.2  
         **end**  
     **end**  
     Compute posterior probability  $\pi(\mathcal{G}_{i,k,j}(\mathbf{V}) | \Psi_{i,k,j}^{(C)})^{(r)}$  of random graph variable  $\mathcal{G}_{i,k,j}(\mathbf{V}$  given  $\Psi_{i,k,j}^{(C)}$  at the  $r$ -th sample of edges  $\{g_{s,s'}^{(r)}\}_{s'/>s; s'=2}^{20}$ .  
**end**  
 Use  $\{\pi(\mathcal{G}_{i,k,j}(\mathbf{V}) | \Psi_{i,k,j}^{(C)})^{(r)}\}_{r=1}^{50,000}$  to compute  $D_H(\mathcal{G}_{i,k,j}(\mathbf{V}), \mathcal{G}_{i,k,j-1}(\mathbf{V}))$  using Equation 3.4, and  $D_{KL}(\mathcal{G}_{i,k,j}(\mathbf{V}), \mathcal{G}_{i,k,j-1}(\mathbf{V}))$  using Equation 3.5.  
 Compute  $MRS_{i,k}^{(Hell)}(j) = D_H(\mathcal{G}_{i,k,j}(\mathbf{V}), \mathcal{G}_{i,k,j-1}(\mathbf{V})) + MRS_{i,k}^{(Hell)}(j-1)$  and  $MRS_{i,k}^{(KL)}(j) = D_{KL}(\mathcal{G}_{i,k,j}(\mathbf{V}), \mathcal{G}_{i,k,j-1}(\mathbf{V})) + MRS_{i,k}^{(KL)}(j-1)$ . Here  $MRS_{i,k}^{(\cdot)}(1) := 0$ . Record  $(j, MRS_{i,k}^{(Hell)}(j))$ , and  $(j, MRS_{i,k}^{(KL)}(j))$ .  
 /\* Recovery trajectory using Hellinger distance function is plotted using  $\{(j, MRS_{i,k}^{(Hell)}(j))\}_{j=2}^{N_{i,k}^{(max)}}$  and using KL divergence is plotted using  $\{(j, MRS_{i,k}^{(KL)}(j))\}_{j=2}^{N_{i,k}^{(max)}}$ . \*/  
**Algorithm 1:** Algorithm for the computation of recovery trajectory for the  $i$ -th patient who plays the  $k$ -th exergame, on  $N_{i,k}^{(max)}$  successive instances.

- except, as we will notice in the results, these points do not offer meaningful information.

GAME	PATIENT ID													Total sessions by game
	3085	3070	3147	3071	3311	3327	3431	3462	3430	3165	3379	3011	3084	
Airplane	26		26	6		20				1				79
Animals	12		8	13			21			3				57
Atlantis	24	55		10		20				2				111
Catch	76	55	53	48	35	32	26	24	22	7	4			382
Color Blocks	12		25											37
Color Clouds	15		12							1				28
Firefly	24	55		10	35	32	26	22	22	1	2			229
Flight Control										1				1
Follow	52		27	40	35	32	26	22	22	1	2			259
Forest Leaves	28		8											36
Izzy the Bee	26	58	12	38	17	12	26	24	22	7	2	3		247
Jugger	76	56	53	48	35	32	26	25	22	1	1			375
Matchday Striker	40		26	19	18					4				107
Nimble	75	57	35	48	35	31	26		22	1	1	1		332
Piano	15		24	18						1				58
Seasons			25											25
Space Ship	35	58	11	24	35	12	26	23	22	2	2	1	1	252
Star Find			26	19						1				46
Total sesions by subject	536	394	371	341	245	223	182	161	154	34	14	5	1	2661

Fig 2: Sessions played by each subject for each of the 18 games.

hipcentre	spine	head	...	shouldercentre
1.684013855	1.680728421	1.694426789	...	1.694013087
1.687542467	1.680152844	1.689994086	...	1.690999615
1.688034792	1.680716982	1.6897329	...	1.692213936
1.688174173	1.680867813	1.690434507	...	1.69244093
1.688240062	1.680919118	1.690826397	...	1.692456947
1.688247039	1.681416153	1.690978133	...	1.693617492
1.688279093	1.681536837	1.691291841	...	1.693789355
1.688287023	1.681549649	1.691346302	...	1.69374882
1.688258504	1.681548505	1.691332804	...	1.693702386
1.688319709	1.681569607	1.691362489	...	1.693638131
...	...	...	...	...

TABLE 1

An excerpt of the first few lines of the 20-columned time series data on locations of the 20 joints of the body recorded at different time points, as Patient 3071 played the exergame Airplane.

## 5. Learning the recovery trajectories

In order to accomplish the learning of the recovery trajectories of patients whose exergame playing performance is recorded on the e-platform *MIRA*, we will first learn the graph of the time series data (on joint-locations) generated as a patient plays an exergame. Thereafter, we will compute the inter-graph distance/divergence between the posterior probabilities of the pair of graphs that are learnt given the time series data on the 20 joint-locations, generated between two successive instances of playing the exergame. We will estimate the correlation

structure of such a time series dataset, and then, conditional on that, we will compute the closed-form marginal posterior of any edge of the graph variable, (see Equation 3.2) to enable sampling from such a marginal.

### 5.1. Computing correlation and partial correlation

To define the inter-column correlation matrix  $\Sigma_{i,k,j}^{(C)}$ , we compute the unbiased estimate of the correlation between each pair of columns of the time series data on the 20 join-locations. Thus, this inter-column correlation matrix is  $20 \times 20$ -dimensional. We will then transform each estimated correlation to the partial correlation, using Eqn. 3.1, to compute the partial correlation matrix  $\Psi_{i,k,j}^{(C)}$ . Below, we present an excerpt of the inter-column (i.e. the inter-joint-location) correlation matrix estimated from the time series data generated by Patient 3071 playing *Airplane*, i.e.

$$\Sigma_{3071, Airplane, 1}^{(C)} = \begin{bmatrix} 1 & 0.330917541 & -0.26122886 & \dots & -0.165895188 \\ 0.330917541 & 1 & 0.68856342 & \dots & 0.870462199 \\ -0.26122886 & 0.68856342 & 1 & \dots & 0.874589366 \\ -0.319381464 & 0.544254133 & 0.692496065 & \dots & 0.730793308 \\ -0.022265821 & 0.128763652 & 0.183350249 & \dots & 0.151056752 \\ 0.16721271 & -0.094951013 & 0.02250426 & \dots & -0.164855981 \\ -0.051876216 & -0.138002972 & -0.006260628 & \dots & -0.100540177 \\ \vdots & \vdots & \vdots & \ddots & \vdots \\ -0.165895188 & 0.870462199 & 0.874589366 & \dots & 1 \end{bmatrix}$$

Then using this inter-joint-location correlation matrix, we compute the partial correlation matrix  $\Psi_{3071, Airplane, 1}^{(C)}$ , as:

$$\Psi_{3071, Airplane, 1}^{(C)} = \begin{bmatrix} 1 & 0.229345539 & -0.150743042 & \dots & -0.201536622 \\ 0.229345539 & 1 & -0.12561909 & \dots & 0.941688165 \\ -0.150743042 & -0.12561909 & 1 & \dots & 0.299565913 \\ 0.041884517 & 0.13053044 & 0.210506791 & \dots & -0.023659251 \\ 0.024567646 & 0.052365098 & -0.128422074 & \dots & -0.018381679 \\ 0.067497723 & 0.002226935 & 0.259867599 & \dots & -0.070459859 \\ -0.096152059 & -0.023513329 & -0.111474649 & \dots & 0.069071476 \\ \vdots & \vdots & \vdots & \ddots & \vdots \\ -0.201536622 & 0.941688165 & 0.299565913 & \dots & 1 \end{bmatrix}$$

### 5.2. Rejection Sampling of an edge from the edge marginal

We draw 50,000 samples of the edge variable  $G_{s,s'}$  that joins the  $s$ -th and  $s'$  nodes of the random graph variable, where the  $s$ -th node of this RGG is

associated with the location of the  $s$ -th joint in the body of the patient, as they play an exergame; ( $s = 1, \dots, 20$ ). The edge  $G_{s,s'}$  is sampled from its closed-form marginal posterior  $m(G_{s,s'} | \psi_{s,s'})$  that is articulated in Equation 3.2, and the sampling is performed using Rejection Sampling. The binary edge variable  $G_{s,s'}$  attains a value  $g_{s,s'}^{(r)}$  in the  $r$ -th sample.

In our implementation of Rejection Sampling, we use a Uniform proposal density, (while we have experimented with a Bernoulli proposal as well), and we accept the proposed edge if and only if the acceptance ratio exceeds or equals  $u$  where  $U = u$ , with the Uniform random variable  $U \sim U[0, 1]$ . The acceptance ratio of the  $r$ -th iteration is

$$\frac{m(g_{s,s'}^{(r)} | \psi_{s,s'})}{Cq(s, s')},$$

with the constant  $C$  chosen to ensure that  $Cq(s, s') \geq m(G_{s,s'} | \psi_{s,s'})$ , such that Rejection sampling is valid. Details of the aforesaid experimentation with the alternate Bernoulli proposal density are discussed in Section 6.3.

For the example case of the patient with ID3071, playing the game *Airplane* 6 times, we use Rejection sampling to draw a sample of size 50,000 of the edge variable  $G_{s,s'}$ ,  $\forall s' > s; s = 1, 2, \dots, 19$ , on each of the 6 instances. In other words, we learn realisations of the graph variable using the time series (on joint locations) data generated by this patient playing this exergame on these 6 occasions.

### 5.3. Inter-graph distance and recovery trajectories: implementation details

For the  $i$ -th patient playing the  $k$ -th exergame on the  $j$ -th instance, we compute the posterior  $\pi(\mathcal{G}_{i,k,j}(\mathbf{V}) | \mathbf{D}_{i,k,j})$  of the random graph variable given the time series (on joint locations) data  $\forall j = 1, \dots, N_{i,k}^{(max)}$ . Then we compute the inter-graph distance/divergence between this posterior of the graph variable learnt using the data generated for the  $j$ -th instance, and that using the data obtained from this patient playing this exergame on the  $(j - 1)$ -th instance,  $\forall j = 2, \dots, N_{i,k}^{(max)}$ . Such inter-graph distance/divergence is computed in accordance with the methodology discussed in Section 3.8.

Table 2 shows the Hellinger distance and Kullback-Leibler divergence between the posterior of the graph variable given the partial correlation structure of the time series data generated when the patient with ID3071 plays the exergame *Airplane* on six successive instances. Table 3 shows the corresponding MRSs that are computed using the distance/divergence, using the methodology discussed in Section 3.9 together with the points originally assigned by the e-platform *MIRA*.

Successive instance pairs	Hellinger distance	Kullbeck-Leibler Divergence
(1,2)	0.10604219	0.10995603
(2,3)	0.10589288	2.5307512e-5
(3,4)	0.0040824151	2.4243133e-6
(4,5)	0.017579886	2.3849898e-3
(5,6)	0.022596656	1.1390906e-3

TABLE 2

*Hellinger distance and Kullbeck-Leibler divergence between posteriors of the random graph variable learnt on successive instances, given time series (on joint locations) data generated by patient with ID3071 playing the exergame Airplane on six instances.*

Instance	MRS via Hellinger	MRS via KL	Points/scores assigned by e-platform <i>MIRA</i>
1	0.05302109	0.05497801	230
2	0.15906328	0.16493404	255
3	0.26495617	0.16495935	290
4	0.26903858	0.16496177	360
5	0.28661847	0.16734676	395
6	0.30921512	0.16848585	315

TABLE 3

*MRS calculated using the Hellinger distance and KL Divergence displayed in Table 2, and points assigned by e-platform *MIRA*, for patient with ID3071 playing the exergame Airplane on six instances*

We visualise the recovery trajectories as the variation of the computed MRS against the index of the instance, when a given patient plays a given exergame. Here, the MRS is computed using either the Hellinger distance or the KL divergence, as per Section 3.9. We also compare our learnt MRS - and thereby the learnt recovery trajectory - against the points that are assigned by the e-platform, across instances in which a game is played. Figure 3 shows examples of these recovery trajectories for patient with ID3071, playing the exergame *Airplane* on six occasions.

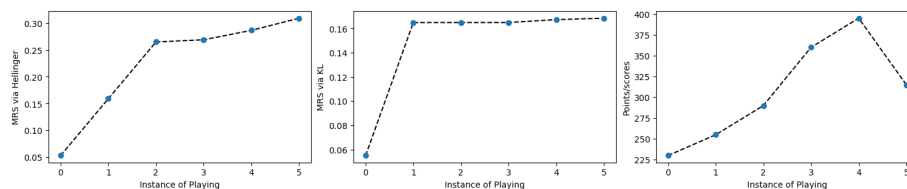


Fig 3: Figure displaying plots of performance of patient ID3071 playing the exergame *Airplane*, against the index of the instance of playing this exergame. On the left, the plot of MRS computed using Hellinger distance is plotted against the index of the instance of playing. In the middle panel, the MRS computed using Kullback-Leibler divergence is plotted, while on the right, points assigned by the *MIRA* e-platform for playing the game on 6 instances, are plotted against the instance index.

## 6. Results

In this section, we report the results obtained from computing values of the parameter that embodies all relevant information about the differences between two disparately-long multivariate time-series datasets on 20 monitored joints of a patient's skeletal framework, produced as the patient plays an exergame, on successive instances. Our parametrisation of such differences between a pair of such successively produced time series datasets, informs on the progress of the patient in recovering their movement ability between such successive playing of the exergame. Above, we have discussed the conceptualisation of this parametrisation as the distance/divergence between the posterior probabilities of random graphs that are learnt given the respective time series data. We conduct such inter-graph distance computation relevant to each patient in the cohort, playing each of the games on successive instances. As discussed in Section 5, we will compute this inter-graph distance for each pair of graphs - learnt given the successive pairs of time series data - to ultimately construct a recovery trajectory for each patient playing an exergame.

### 6.1. Realisations of the graph variable at chosen $\tau$

In Figure 4 we present the realisations of the graph variable, learnt at a  $\tau$  of 0.2, given the time series (on joint locations) datasets that are produced, as patient ID3071 plays *Airplane* on six different instances. Realisations learnt at  $\tau = 0.3$ , given data produced by the patient ID3311 playing exergame *Follow*, are presented in Figure 5.

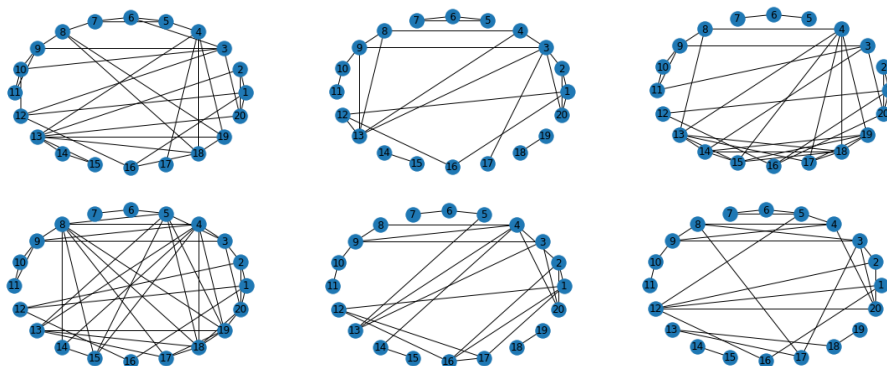


Fig 4: Realisations of graphs learnt at a chosen  $\tau$  of 0.2, given data recorded for patient ID3071 playing exergame *Airplane* on six successive instances, in the order of the instance of playing.

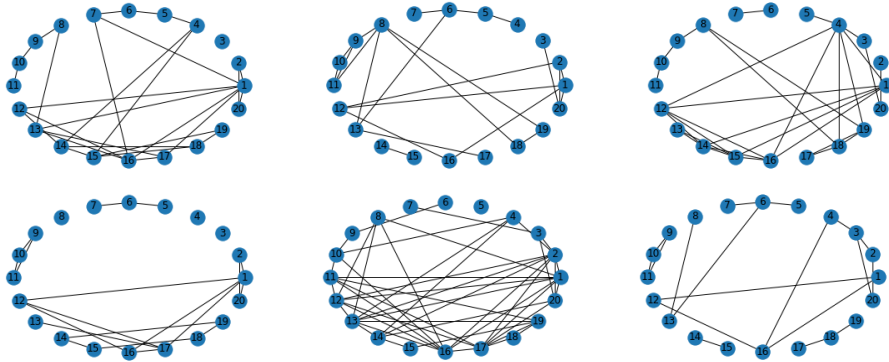


Fig 5: Realisations of the graph variable, learnt at  $\tau = 0.3$ , given data recorded for the patient ID3311 playing exergame *Follow*, on 35 successive instances - of which, results of playing on 6 instances are presented here, in the order of the instance of playing.

## 6.2. Recovery Trajectories and MRS

Having learnt the posteriors of the graph variable given the time series (on joint locations) data generated by the  $i$ -th patient playing the  $k$ -th exergame, on all relevant instances, we proceed to construct the recovery trajectories for this patient, as they play a given exergame. The following figures show the evolution in the learnt MRS as the patient repeatedly plays an exergame, across all instances of playing it. In Figure 6 and Figure 7 we display recovery trajectories of the patient ID3085 playing the exergame *Catch* 76 times, and the patient ID3327 playing exergame *IzzytheBee* 12 times. For each patient, we show the comparison of the rate of change of MRS, and the MRS - computation of which is discussed in Section 3.9 - using the Hellinger distance function; KL divergence; as well as the scores (points gained at the end of playing an exergame) provided by *MIRA*.

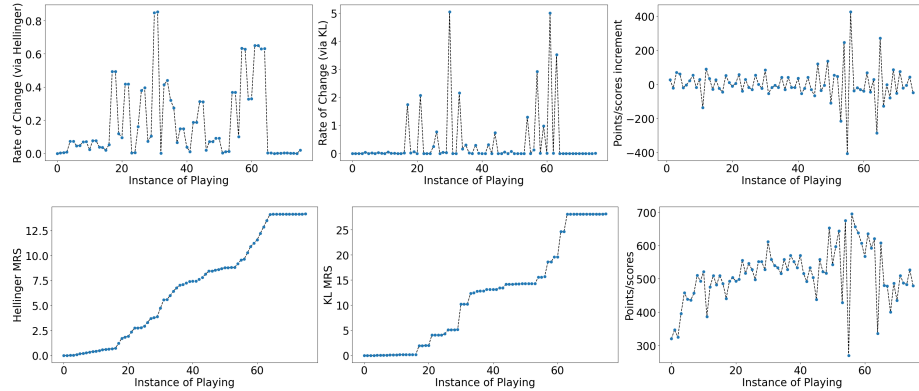


Fig 6: Results for the patient with ID3085, playing the exergame *Catch*, 76 times. The panels in the first row display plots of rate of change of MRS (left and middle) and that of the points assigned by the e-platform *MIRA* (right) at various instances. The panels in the bottom row display the MRS (left and middle) and the points assigned by *MIRA*. In the first column, Hellinger distance has been employed to compute the distance between posteriors of the graph variables learnt using data generated at successive instances of playing the exergame. The second column is similar to the first, except here, results are shown for the inter-graph divergence computed using the Kullback-Leibler divergence.

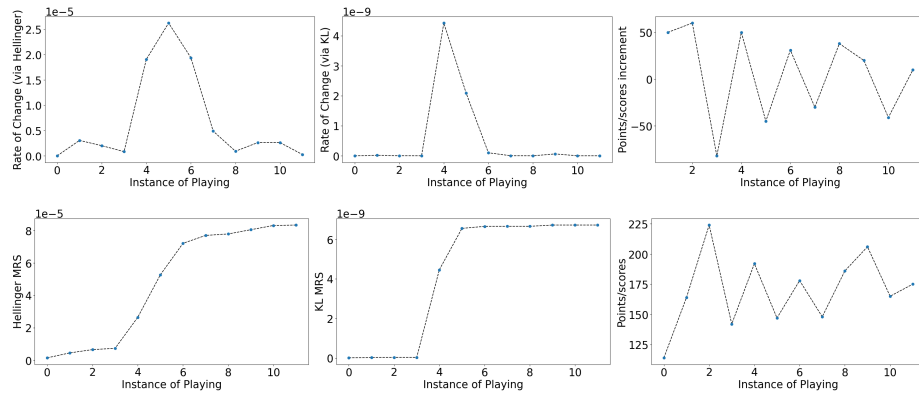


Fig 7: Same as for Figure 6, with results displayed for the patient ID3327 playing the exergame *IzzytheBee* 12 times.

From Figure 6 and Figure 7, it can be seen that MRSs computed using Hellinger/Kullbeck-Leibler, represent clearly visualised recovery trajectories,

based on robust learning of the performance indicator of recovery. Indeed, this learning is robust to variation in the number of instances of playing an exergame, as well as in the time taken for a patient to play an exergame.

**Remark 6.1.** *Evolution of the points provided by the e-platform MIRA does not offer a meaningful trend. Instead, the inbuilt point assignment facility on MIRA offers wide variations in the performance indicator. Thus, the feedback on recovery offered on the basis of the points assigned by MIRA, is far less clear than that provided by MRS values.*

It is worth noting that the level of difficulty of the exergames changes over time, giving rise to a temporary depression in performance, when the patient moves to a harder level.

In general, recovery trajectories computed using the Hellinger distance and KL divergence measures, roughly agree with each other. However by the definition of distance, the Hellinger distance will yield the absolute of the difference between the scores attained by a patient when playing a game on two successive instances; therefore, the MRS computed using the Hellinger distance measure is never smaller on one instance, compared to the MRS computed at the previous instance. On the other hand, the Kullback-Leibler divergence allows a negative value for the divergence between the posteriors of graph models learnt using (partial correlation of) the joint-location time series data generated on successive instances of playing a game - which is the rate of change in the MRS between the two successive instances. Therefore, the MRS computed using the KL divergence function on one instance can be smaller than that in the previous. Then it follows that the recovery trajectory learnt using the KL divergence measure will not adhere to local monotonicity, (as noted in the recovery trajectories of the subject ID3147 playing game *Follow*, the subject ID3327 playing game *Nimble* and so on).

**Remark 6.2.** *We find it an informative result that most of the recovery trajectories learnt with both the distance and divergence measures concur, indicating that most of the patients in the cohort, avail of improving movement ability, with increasing instances of playing the game.*

**Remark 6.3.** *In applications to learning recovery trajectories using generic datasets, we recommend the usage of KL-divergence over Hellinger distance, based only on the criterion that the KL-divergence can produce both positive and negative rates of change of the MRS, while such a rate is essentially positive when the MRS is computed using the Hellinger distance function.*

### 6.3. Robustness of the graph learning

We checked for the robustness of graph learning to variation in the proposal density used in the undertaken Rejection Sampling, by learning the recovery trajectories of the patient ID3071, playing the game *Airplane* on six instances, using both a Bernoulli and a Uniform proposal in our implementation of Rejection sampling. For this example case, we drew a sample of size 500,000 for

$g_{s,s'}, \forall s' > s; s = 1, 2, \dots, 19$ , once with a *Bernoulli*( $|\psi_{s,s'}|$ ) proposal, and separately, with a *Uniform*[0, 1] proposal. We computed the inter-graph distance thereafter, to ultimately learn the recovery trajectories. The learnt trajectories are plotted in Figure 8 for inter-graph distance learnt using the Hellinger distance measure and the KL divergence measure. Near-concurrence of the learnt trajectories testify to the robustness of our learning to changes in details of the undertaken Rejection Sampling.

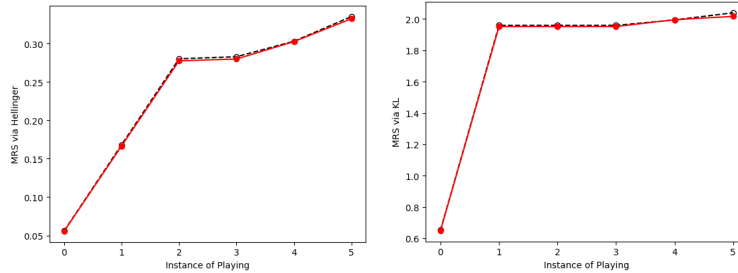


Fig 8: Comparison of recovery trajectories of patient ID3071 playing the exergame *Airplane* on 6 instances, learnt using Uniform proposal (in black dashed lines and unfilled circles) and Bernoulli proposal (in red - or grey in the monochromatic version of the articles - solid lines and red circles). Results using the Hellinger distance function are displayed in the left panel while results using KL-divergence are shown on the right.

#### 6.4. More Recovery Trajectories

Figure 9 presents a collection of more recovery trajectories learnt for different patients playing different exergames, multiple times, using MRS computed using the Kullback-Leibler divergence measure.

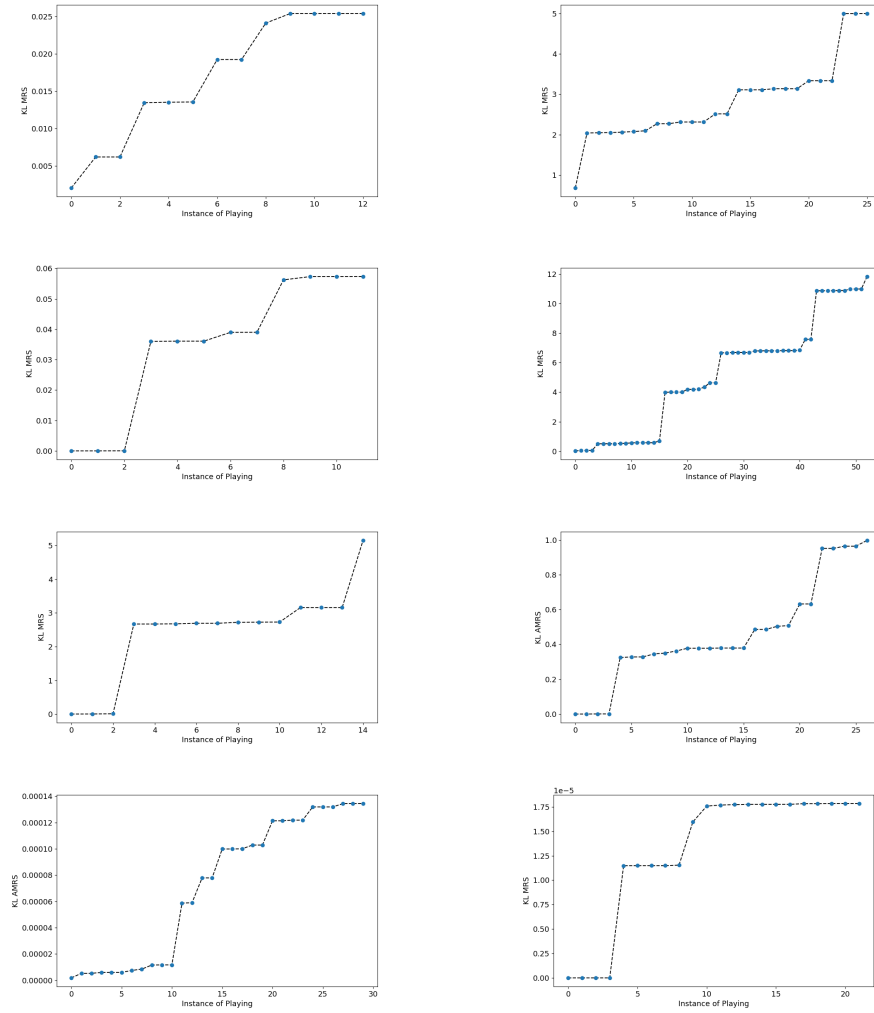


Fig 9: Recovery trajectories of patients, computed using KL.

In general, from our calculated recovery trajectories, most of the patients show an improvement in the physical rehabilitation during the training (which is not that evident from the statistics provided by *MIRA* platform). This finding is also supported by the MRI profile scans and patient functional assessment taken at the beginning and the end of the training programme that showed significant improvement in motor function [37]. Our method provides an easy way to visualise and interpret the recovery information of such patients.

### 6.5. Discussion of results

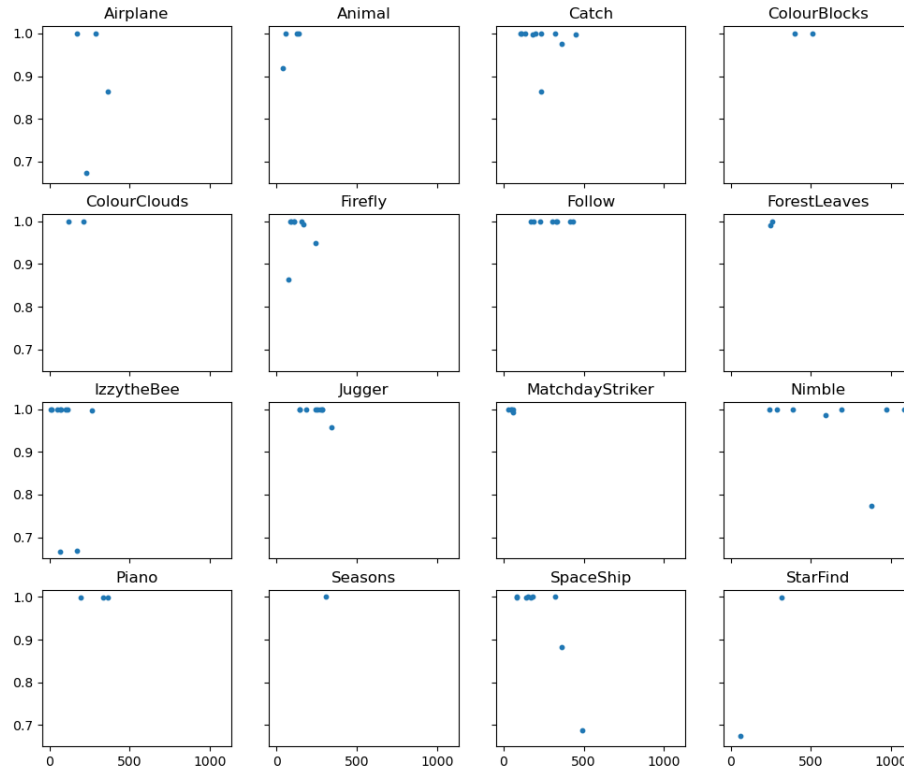


Fig 10: Plots of computed recovery parameter of all patients playing a particular exergame, (noted in the panel header), against the points scored by a patient on the MIRA e-platform, in the first instance that they play the considered exergame. The recovery parameters are plotted only for those patients who played this exergame in at least four instances

We now collate the results of learning recovery trajectories for this cohort of patients, to advance recommendations as to the “best” suited exergame for a patient with a given level of mobility-impediment at the stage when the physical rehabilitation programme is just about to begin. This calls for the identification of the pre-rehab mobility level, and of a (scalar-valued) parameter that measures recovery. We discuss these below.

- The best proxy for the pre-rehab mobility level of the  $i$ -th patient is the automated score  $\mathcal{S}_{i,k}(1)$  that they obtain on the e-platform *MIRA*, when undertaking the  $k$ -th exergame in the first instance of playing this exergame. The lower is  $\mathcal{S}_{i,k}(1)$ , the higher is the mobility impediment faced by the  $i$ -th patient.

- The recovery trajectory itself is the most appropriate recovery measure, but it is a vector-valued variable (that approximates a function). Here, we implement the recovery trajectory that results from the MRS computed using the KL-divergence measure. We use such a recovery trajectory to compute the scalar-valued recovery parameter  $\alpha_{i,k}$  of the  $i$ -th patient playing the  $k$ -th exergame, as the (normalised) range of such MRS values attained by this patient over the full course of them playing this exergame:

$$\alpha_{i,k} := \frac{\mathcal{MRS}_{i,k}^{(KL)}(N_{i,k}^{(max)}) - \mathcal{MRS}_{i,k}^{(KL)}(2)}{\mathcal{MRS}_{i,k}^{(KL)}(N_{i,k}^{(max)})}.$$

We then plot  $\alpha_{i,k}$  against  $\mathcal{S}_{i,k}(1)$ , for all those patients who played the  $k$ -th game at least four times. The plots for the 16 relevant exergames, *Airplane*, *Animal*, *Catch*, *ColourBlocks*, *ColourClouds*, *Firefly*, *Follow*, *ForestLeaves*, *IzzytheBee*, *Jugger*, *MatchdayStriker*, *Nimble*, *Piano*, *Seasons*, *SpaceShip*, *StarFind* are shown for 10 patients in Figure 10. There are two points that need to be appreciated:

1. between two exergames, the one that demonstrates a higher recovery parameter at lower initial scores, (i.e. for more severe mobility impediment), is the more efficient of the two;
2. we can use this figure to suggest the “best” exergames for patients with a given level of severity of mobility difficulties, as parametrised by the initial score.

From point 1 above, in the cohort we have analysed, the exergames with the highest rehabilitating proficiencies are: *IzzytheBee*; *MatchdayStriker*; *Animal* - in that order. Again, in this data, the exergames *Catch*; *Follow*; *Jugger* appear to be the ones that are nearly equally proficient in rehabilitating patients across a wide range of severity of mobility impediments. However, *Nimble* appears to be a game with little discretionary capacity - all patients, irrespective of their initial level of mobility deficiency, appear to attain high recovery upon playing this exergame. So *Nimble* is not recommended as a suitable exergame.

So a patient who suffered from severe mobility impediment at the start of their rehab programme - on the basis of the information that we have at hand - is best recommended to play *IzzytheBee*; *MatchdayStriker*; *Animal*, and perhaps *Firefly* and *Spaceship* as well. For those with less severe impediments, *Catch*; *Follow*; *Jugger* are more suitable. Those with the least severe difficulties are recommended to play *ColourBlocks*; *Catch*; *Follow*.

It is worth mentioning that our approach could be both applied to any different similar platform or could be expanded beyond a virtual reality platform, to a simple set of exercises that could be done in a home environment.

## 7. Conclusions

Our method of learning recovery trajectories allows for patient-specific recommendations of the optimal route for rehab, where said recommendations are

provided at an early stage, (i.e. before the physical rehab has started). In a future contribution, we will be undertaking the prediction of the full recovery trajectory of an individual patient. To perform such a prediction, the pre-requisite is a training dataset that would permit the (supervised) learning of the relation between pre-rehab severity of mobility impediment in an individual patient, and the recovery trajectory that marks this patient's recovery as they play the  $k$ -th exergame, where  $k$  indexes any of the exergames marked in Figure 10. Such a supervised learning will enable the prediction of the recovery trajectory for a patient with a given level of mobility impairment, at the start of the therapeutic programme. Such a prediction will offer physicians and therapists a robust patient-specific and early assessment of a given patient's course of recovery. Already with the results reported here, we offer robust recommendations about the optimal exergames suitable for a patient with categorised severity, where severity at the pre-rehab stage above, is proxied by the patient's initial score that is recorded (in an automated way) on the e-platform *MIRA* as the patient plays the exergame in question. In general applications, the initial state of mobility impediment could be informed upon otherwise/additionally as well.

We note that our learning of the recovery trajectories is founded on rigorous mathematics, namely on the statistical distance/divergence between random graph variables that are learnt given respective data slices. Each such dataset comprises a time series of locations of 20 joints of the patient's skeletal frame, recorded while the patient undertakes an exergame on various instances. Then the distance between the graphs learnt given data generated on playing at the current instance and the previous, allows for the computation of the MRS relevant to the current instance.

We forward this method as one that is relevant to the wider and topical quest for early and patient-specific diagnosis. Additionally, this automated protocol is easy to implement and is suitable for small cohort sizes; prediction of the optimal exergame is fast; and crucially, the learning of recovery trajectories by this method is robust and explainable. Given recent developments in the identification of the "optimal"  $\tau$  in a given dataset, in a future contribution, we will compute the distance/divergence between two RGG variables that are learnt given the correlation structure of the respective datasets, using the identified optimal  $\tau$  values in the relevant dataset.

## References

- [1] Valery L Feigin, Michael Brainin, Bo Norrving, Sheila Martins, Ralph L Sacco, Werner Hacke, Marc Fisher, Jeyaraj Pandian, and Patrice Lindsay. World Stroke Organization (WSO): Global stroke fact sheet 2022. *Int J Stroke*, 17(4):479, 2022.
- [2] World Health Organization. International classification of functioning, disability and health(ICF), 2001.
- [3] David Walton. A review of the definitions of 'recovery' used in prognostic studies on whiplash using an icf framework. *Disabil Rehabil*, 31(12):943–957, 2009.

- [4] Carrie Ritchie and Michele Sterling. Recovery pathways and prognosis after whiplash injury. *J Orthop Sports Phys Ther*, 46(10):851–861, 2016.
- [5] Petrina P Casey, Anne Marie Feyer, and Ian D Cameron. Course of recovery for whiplash associated disorders in a compensation setting. *Injury*, 46(11):2118–2129, 2015.
- [6] H Kasch, F W Bach, and T S Jensen. Handicap after acute whiplash injury: a 1-year prospective study of risk factors. *Neurology*, 56(12):1637–1643, 2001.
- [7] Dejan Ozegovic, Linda J. Carroll, and J. David Cassidy. Does expecting mean achieving? the association between expecting to return to work and recovery in whiplash associated disorders: a population-based prospective cohort study. *Eur Spine J*, 18(6):893–899, 2009.
- [8] Daniel S Nagin. Analyzing developmental trajectories: A semiparametric, group-based approach. *Psychological Methods*, 4:139–157, 1999.
- [9] Bengt Muthén and Linda K. Muthén. Integrating person-centered and variable-centered analyses: Growth mixture modeling with latent trajectory classes. *Alcoholism: Clinical and Experimental Research*, 24(6):882–891, 2000.
- [10] Daniel S Nagin. *Group-Based Modeling of Development*. Harvard University Press, Cambridge, Massachusetts, United States, 2005.
- [11] David M. Walton, Dan Krebs, Dianna Moulden, Peter Wade, Lenerdene Levesque, James Elliott, and Joy C. Macdermid. The traumatic injuries distress scale: A new tool that quantifies distress and has predictive validity with patient-reported outcomes. *Journal of Orthopaedic and Sports Physical Therapy*, 46(10):920–928, 2016.
- [12] Francisco J. Herrera, Jean Wong, and Frances Chung. A systematic review of postoperative recovery outcomes measurements after ambulatory surgery. *Anesthesia and Analgesia*, 105(1):63–69, 2007.
- [13] Peter A. Stark, Paul S. Myles, and Justin A. Burke. Development and psychometric evaluation of a postoperative quality of recovery score: The QoR-15. *Anesthesiology*, 118:1332–1340, 2013.
- [14] Colin F. Royse, Stanton Newman, Frances Chung, Jan Stygall, Rachel E. McKay, Joachim Boldt, Frederique S. Servin, Ignacio Hurtado, Raafat Hannallah, Buwei Yu, and David J. Wilkinson. Development and feasibility of a scale to assess postoperative recovery: The post-operative quality recovery scale. *Anesthesiology*, 113:892–905, 2010.
- [15] Tony Jung and K. A. S. Wickrama. An introduction to latent class growth analysis and growth mixture modeling. *Social and Personality Psychology Compass*, 2(1):302–317, 2008.
- [16] Nilam Ram and Kevin J. Grimm. Growth mixture modeling: A method for identifying differences in longitudinal change among unobserved groups. *International Journal of Behavioral Development*, 33(6):565–576, 2009.
- [17] Guus Panken, Trynke Hoekstra, Arianne Verhagen, Maurits van Tulder, Jos Twisk, and Martijn W Heymans. Predicting chronic low-back pain based on pain trajectories in patients in an occupational setting: an exploratory analysis. *Scand J Work Environ Health*, 42(6):520–527, 2016.

- [18] Joshua Y. Lee, David M. Walton, Paul Tremblay, Curtis May, Wanda Millard, James M. Elliott, and Joy C. MacDermid. Defining pain and interference recovery trajectories after acute non-catastrophic musculoskeletal trauma through growth mixture modeling. *BMC Musculoskelet Disord*, 21(1), 2020.
- [19] David M. Walton, James M. Elliott, Joshua Lee, Mohamad Fakhereddin, and Wonjin Seo. Identification of clinically-useful cut scores of the traumatic injuries distress scale (TIDS) for predicting rate of recovery following musculoskeletal trauma. *PLoS ONE*, 16(3), 2021.
- [20] Samuel I. Daitch, Jonathan A. Kelner, and Daniel A. Spielman. Fitting a graph to vector data. In *Proceedings of the 26th Annual International Conference on Machine Learning, ICML '09*, page 201–208, New York, NY, USA, 2009. Association for Computing Machinery.
- [21] Xiaojin Zhu, Zoubin Ghahramani, and John D Lafferty. Semi-supervised learning using gaussian fields and harmonic functions. In *Proceedings of the 20th International conference on Machine learning (ICML-03)*, pages 912–919, 2003.
- [22] Esther B Olasoji, Daniel K Uhm, Oluwole O Awosika, Sylvain Doré, Carolyn Geis, and Alexis N Simpkins. Trends in outpatient rehabilitation use for stroke survivors. *Journal of the neurological sciences*, 442:120383, 2022.
- [23] Reza Haghighi Osgouei, David Soulsby, and Fernando Bello. Rehabilitation exergames: Use of motion sensing and machine learning to quantify exercise performance in healthy volunteers. *JMIR Rehabil Assist Technol*, 7(2):e17289, 2020.
- [24] Sadawi Nouredin, Miron Alina, Ismail Waidah, Hussain Hafez, and Grosan Crina. Gesture correctness estimation with deep neural networks and rough path descriptors. *2019 International Conference on Data Mining Workshops (ICDMW)*, pages 595–602, 11 2019.
- [25] Marianna Capecci, Maria Gabriella Ceravolo, Francesco Ferracuti, Sabrina Iarlori, Andrea Monteriu, Luca Romeo, and Federica Verdini. The kimore dataset: Kinematic assessment of movement and clinical scores for remote monitoring of physical rehabilitation. *IEEE Transactions on Neural Systems and Rehabilitation Engineering*, 27(7):1436–1448, 2019.
- [26] Adeline T M Paiement, Lili Tao, Sion L Hannuna, Massimo Camplani, Dima Damen, and Majid Mirmehdi. Online quality assessment of human movement from skeleton data. *Proceedings of the British Machine Vision Conference 2014*, 2014.
- [27] Fotos Frangoudes, Maria Matsangidou, Eirini C. Schiza, Kleantlis C. Neokleous, and Constantinos S. Pattichis. Assessing human motion during exercise using machine learning: A literature review. *IEEE Access*, 10:86874–86903, 2022.
- [28] MIRA Rehab. <https://www.mirarehab.com/>.
- [29] E. N. Gilbert. Random plane networks. *Journal of the Society for Industrial and Applied Mathematics*, 9(4):533–543, 1961.
- [30] Alexander P Giles, Carl P Dettmann, and Orestis Georgiou. Connectivity of soft random geometric graphs over annuli. *J Stat Phys*, 162:1068–1083,

- 2016.
- [31] Mathew D Penrose. Connectivity of soft random geometric graphs. *The Annals of Applied Probability*, 26(2):986–1028, 2016.
  - [32] D. Chakrabarty, K. Wang, A. Roy, G. and Bhojgaria, C. Zhang, J. Pavlu, and J. Chakrabartty. Constructing training set using distance between learnt graphical models of time series data on patient physiology, to predict disease scores. *PloS one*, 18(10):e0292404, 2023.
  - [33] B. Schweizer and A. Sklar. *Probabilistic Metric Spaces*. Dover Publications, 2011.
  - [34] D. Chakrabarty. *Learning in the Absence of Training Data*. Springer International Publishing, 2024.
  - [35] R. van der Hofstad. *Random Graphs and Complex Networks: Volume 2*. Cambridge Series in Statistical and Probabilistic Mathematics. Cambridge University Press, 2024.
  - [36] Florence Regol, Soumyasundar Pal, Jianing Sun, Yingxue Zhang, Yanhui Geng, and Mark Coates. Node copying: A random graph model for effective graph sampling. *Signal Process.*, 192(C), mar 2022.
  - [37] Younis M. S. Firwana, Mohd Khairul Izamil Zolkefley, Hasnetty Zuria Mohamed Hatta, Christina Rowbin, Che Mohd Nasril Che Mohd Nasir, Muhammad Hafiz Hanafi, Mohd Shafie Abdullah, Bilgin Keserci, Natasha A. Lannin, and Muzaimi Mustapha. Regional cerebral blood perfusion changes in chronic stroke survivors as potential brain correlates of the functional outcome following gamified home-based rehabilitation (intel-lirehab)—a pilot study. *Journal of NeuroEngineering and Rehabilitation*, 19(1):94, 2022.